tvst

https://doi.org/10.1167/tvst.7.1.8

Article

Three Dimensional Stimulus Source for Pattern Electroretinography in Mid- and Far-peripheral Retina

Shresta Patangay[1], Zahra Derafshi[1], Thasarat S. Vajaranant[2], Jason C. Park[2], Elham Ghahari[2], J. Jason McAnany[2], and John R. Hetling[1]

[1] Department of Bioengineering, University of Illinois at Chicago, Chicago, IL, USA
[2] Department of Ophthalmology and Visual Sciences, University of Illinois at Chicago, Chicago, IL, USA

Correspondence: John R. Hetling, Department of Bioengineering, University of Illinois at Chicago, 851 S Morgan St, Chicago, IL 60607-7052, USA. e-mail: JHetli1@uic.edu

Received: 14 August 2017
Accepted: 21 November 2017
Published: 19 January 2018

Keywords: electrophysiology; pERG; peripheral retina; ganglion cells

Citation: Patangay S, Derafshi Z, Vajaranant TS, Park JC, Ghahari E, McAnany JJ, Hetling JR. Three dimensional stimulus source for pattern electroretinography in mid and far peripheral retina. Trans Vis Sci Tech. 2018;7(1):8, https://doi.org/10.1167/tvst.7.1.8

Purpose: The pattern electroretinogram (pERG) response reflects, in part, ganglion cell function. However, probing retinal ganglion cell (RGC) function in the mid- and far peripheral retina is difficult with conventional flat-panel pERG stimulus sources. A pattern stimulus source is presented for probing the peripheral retina. Peripheral pERG (ppERG) responses were evaluated versus luminance, reversal rate, and field subtended, and were compared with conventional pERG in healthy eyes.

Methods: Eleven normally-sighted subjects were recruited. A hemispherical surface was used to present a reversing checkerboard pattern to the peripheral retina, from approximately 35° to 85° of visual field, in all directions. Responses to stimuli presented to peripheral field sectors (superior, nasal, inferior, temporal) were also recorded. Conventional pERG responses were recorded on the same day. Amplitudes and implicit times of waveform peaks were evaluated.

Results: Robust pERG responses from peripheral retina resemble conventional pERG responses but with shorter implicit times and reduced positive component. Responses to high-luminance patterns include high-frequency components resembling flash ERG oscillatory potentials. Negative response component amplitudes increased with increasing pattern luminance, and decreased with increasing reversal rate.

Conclusions: Peripheral-field pERG responses are robust and repeatable; the unique response properties reflect differences between central and peripheral retina. Field-sector response ratios can be used to probe for sectoral dysfunction associated with disease.

Translational Relevance: The ppERG approach provides direct measurement of proximal retinal function beyond the fields probed by conventional perimetry and pERG, providing access to a relatively under studied part of the retina relevant to early stage glaucoma.

Introduction

The pattern electroretinogram (pERG) is recorded in response to a reversing high-contrast pattern, typically a checkerboard or grating, which has a constant time-averaged luminance. The pERG response waveform reflects retinal ganglion cell function, as evidenced by a reduced pERG response in glaucoma patients[1–3] as well as in the presence of pharmacologic block of ganglion cells[4–7] or experimental optic nerve transection.[8,9] Because of the strong ganglion cell contribution, the pERG has high-relative efficacy for glaucoma when compared with other electrophysiological tests of visual function.[10,11] In glaucoma, it is well documented that relative changes (compared with age-matched healthy eyes) in pERG amplitude can precede equivalent relative changes in structural measures (retinal nerve fiber layer [RNFL] thinning) or measurable defects in visual field.[12–16] However, despite some use as an outcome measure in clinical research[17,18] the sensitivity and specificity of pERG have not been so high as

to overcome the perceived clinical burden of performing the test for routine screening, diagnosis, or monitoring of disease progression, where Humphrey Visual Field testing (HVF) and optical coherence tomographic imaging (OCT) are typically employed.

In the ERG studies cited above, measurements were made at or near the central retina (centered on the fovea). One issue that may limit the sensitivity of conventional pERG testing in glaucoma is only targeting the central 20° to 30° of visual field. The reported sensitivity of pERG to early, putatively diffuse, ganglion cell dysfunction (prior to detection with other central-field tests) suggests that the locus of the earliest damage may, in some patients, be in the peripheral retina,[13,19] even beyond the commonly observed arcuate scotoma in the Bjerrum area (~10°–20° from fixation). Patients with abnormal sectors in the circumpapillary OCT and normal HVF suggest that the associated functional field defects are beyond the 24° HVF test area.[20] A test of ganglion cell function that probes the peripheral retina could therefore prove more sensitive than central field tests in some cases; this possibility is the motivation for the present study.

Given the advantages of electrophysiologic testing (objective, assesses function), a pERG test that elicits a response dominated by ganglion cell activity in the peripheral retina was developed. Noncentralized pERG stimuli have been proposed as a means of assessing disease in the mid-peripheral retina,[21,22] but standard flat monitor sources are not ideally suited to the task. Therefore, a stimulus source was designed and fabricated that would present a reversing checkerboard pattern to the peripheral retina, spanning approximately 35° to 85° in all directions. This report explores the peripheral-field pERG (ppERG) parameter space (luminance, reversal rate, field probed), describes estimated normal ranges for ppERG responses, and compares ppERG and conventional central-field pERG responses in healthy eyes. These results demonstrate differences between central and peripheral responses to pattern stimuli and motivate further study of ppERG responses in glaucoma, as well as in other diseases affecting inner retinal function in the periphery.

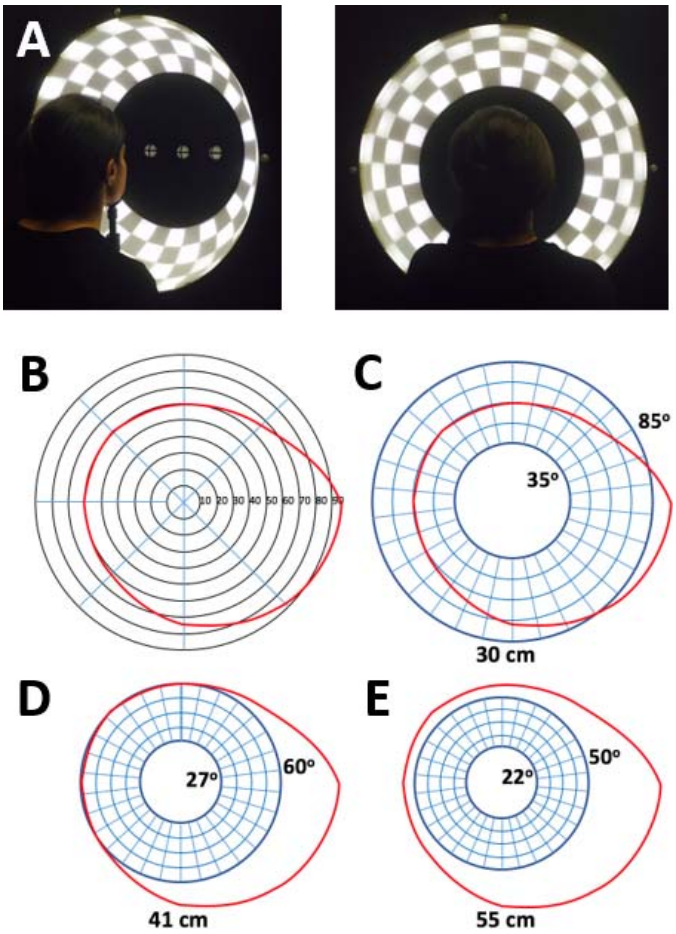

Figure 1. Visual field subtended by the three-dimensional peripheral pattern stimulus source. (A) Two views of a subject at the 30-cm viewing distance (note chin rest in *left panel*); fixation was always at the central target at the apex of the hemisphere. (B) Limits of the visual field for a healthy right eye, indicated by the *red curve*. *Numbers* represent visual angle from direction of gaze (center of grid). (C) Schematic of the ppERG stimulus source as seen from the 30-cm viewing distance, with visual field limits superimposed (*red curve* from panel B). Angular subtense from direction of gaze to the inner and outer margins of the stimulus field are indicated. (D) ppERG stimulus field as seen from the 41-cm viewing distance. (E) ppERG stimulus field as seen from 55-cm viewing distance. Schematics approximately to scale.

Methods

Peripheral Pattern Stimulus Source

The ppERG signal was recorded while the subject viewed a reversing checkerboard presented on a hemispherical surface that filled a substantial portion of the peripheral the visual field (Fig. 1A). Each check was illuminated by a "cool white" light-emitting diode (LED; BXRA-C0402, correlated color temperature of 5600 K, maximum output 450 lumens; Bridgelux, Fremont, CA) behind the translucent hemisphere (30-cm radius, 0.125-inch thick clear acrylic with both surfaces "frosted"); the borders of the checks were defined by thin metal fins perpendicular to the convex surface and were therefore fixed in size. A thin

diffusing element was positioned between each LED and the hemisphere to improve uniformity of luminance within each check. The mean ON-luminance was varied from 90 to 1670 photopic cd m^{-2}; luminance of every check was measured periodically throughout the 2-year study, and LED driving currents adjusted as necessary to maintain calibration. For a given mean ON-luminance, the standard deviation (SD) of luminance across checks was approximately 16%; this larger than desired variation was due to wide manufacturing tolerances of the LEDs. Careful static luminance measurements using a photometer (IL 1700; International Light Technologies, Peabody, MA), and luminance versus time measurements using photodiodes, confirmed equal mean luminance for each phase of the pattern, and an absence of transient luminance artifacts (all-dark or all-bright periods accompanying each pattern reversal), respectively. The four rows and 30 columns formed a spherical section. Subjects were positioned at one of three viewing distances (distance from eye to dome apex, ±1 cm due to variations in face shape) via a moveable chin rest, and a target at the apex of the hemisphere was fixated during recording. The field subtended by the stimulus pattern is illustrated in Figures 1B to 1E, where the limits of visual field for a right eye (red curve) is superimposed on a representation of the ppERG stimulus for each viewing distance used in this study. The physical check size was not adjustable (smallest checks 6.1 × 6.0 cm, largest checks 6.3 × 6.5 cm), and so apparent check size varied with viewing distance; checks were slightly trapezoidal in shape. Average apparent check size, luminance, and reversal rates investigated for the ppERG stimulus source are given in Table 1. At the highest pattern luminance, contrast was measured as 97%. Unless otherwise noted, the conventional pERG system used in this study (Espion E^3 Electroretinography system with pattern stimulus generator; Diagnosys LLC, Lowell, MA) conformed to International Society for Clinical Electrophysiology of Vision (ISCEV) recommended settings,[23] also provided in Table 1. Pattern luminance was not adjusted for pupil size.

Table 1. Parameter Values for the Peripheral Pattern Stimulus Source (ppERG) and Conventional pERG Stimulus Source Used in this Study

	ppERG	pERG
Mean ON-luminance (ph cd m^{-2})	90 160 830 1670	90
Check size	10° at 30 cm 7.5° at 41 cm 5° at 55 cm	1°
Reversal rate	2.3 RPS 4.6 RPS 9.2 RPS	4.0 ± 0.8 RPS
Stimulus field (half angle)	35–85° at 30 cm 27–60° at 41 cm 22–50° at 55 cm	0–15° at 55 cm

pERG stimulus values conform to ISCEV-recommended values.

Subjects

Eleven normally-sighted subjects (15 eyes recorded from) were recruited. Informed consent was obtained from all subjects before participation. Procedures adhered to the tenets of the Declaration of Helsinki, and the protocol was approved by an institutional review board at the University of Illinois at Chicago. The subjects had no history of eye disease, normal visual acuity, RNFL thickness within normal limits (average over all sectors: range, 75–101 μm; mean ± SD, 89 ± 8 μm), and refractive error that ranged from 0 to −5.00 diopters. Subjects ranged in age from 22 to 65 years (mean ± SD, 43 ± 15 years).

ERG Recording

Responses were recorded from one eye in seven subjects, and both eyes in four subjects. With the exception of one subject who wore contact lenses, no corrective lenses were worn during ppERG recording. Eyes received one drop of 0.5% proparacaine HCl, and a DTL fiber electrode (Diagnosys LLC, Lowell, MA) was installed per instructions. Adhesive skin electrodes were used for reference (ipsilateral temple) and ground (neck). Once subjects were seated comfortably at the appropriate distance, room lights were turned off, the reversing pattern was turned on, and the subject was asked to fixate the central target. Recording was done in 5-second epochs, separated by 3- to 4-second rest periods (during which the pattern reversals continued), and 10 to 30 epochs were obtained for each recording condition. Test time for each condition rarely exceeded 3 minutes; up to five recording conditions, with breaks between, were tested for each subject. Signals were amplified (P511 amplifier; Grass Technologies, West Warwick, RI) to a final resolution of 0.122×10^{-3} μV bit^{-1}, 16-bit

analog to digital conversion, and recorded within the passband 1 to 1000 Hz (high pass 2-pole active filter, −12 dB/octave, −6 dB at 1.0 Hz; low pass 4-pole active filter, −24 dB/octave, −6 dB at 1000 Hz), then digitized at 5-kHz sampling rate and stored for later analysis. The ppERG signal was monitored in real time; large artifacts due to blinking were noted and resulted in additional epochs being recorded until at least 200 "clean" pattern reversals were obtained for off-line averaging. Conventional pERG recording was performed according to ISCEV standards,[23] including correction for refractive error, on the same day.

Analysis

ppERG response waveforms evoked with high-luminance patterns were distinct from typical pERG response waveforms obtained using ISCEV-recommended stimulus values. A representative waveform is plotted in Figure 2A. The most apparent novel feature in the ppERG waveform is the series of high-frequency oscillations occurring in the time range of 10 to 45 ms. To evaluate waveform components for amplitude and implicit time, the high-frequency components were isolated from the low-frequency components. Fourth-order Butterworth filters, with pass-bands of 1 to 50 and 50 to 1000 Hz, were applied to the raw waveforms; each filter was applied twice, once forward and once backward, to minimize phase shifts in the filtered data (filtfilt function in MATLAB; MathWorks, Natick, MA). The cutoff frequency of 50 Hz was found to provide the best separation of high- and low-frequency peaks across the recording protocols used here.

The isolated low-frequency waveform (Fig. 2B) typically included an early positive phase and a later negative phase, similar to conventional pERG waveforms (P50 and N95), but with shorter implicit times; they are referred to here simply as P and N. P was measured from baseline to the positive peak; N was measured as the difference between P and the negative trough. The isolated high-frequency waveform (Fig. 2C) typically included three distinct peaks, referred to here as F1, F2, and F3. F1 was measured from baseline to peak; F2 and F3 were measured from the previous trough to peak, analogous to amplitude evaluation of flash ERG oscillatory potentials. All peak and trough amplitudes were evaluated as the maximum or minimum values, respectively, within standard time windows determined by visual examination of the range of peak times across all study participants.

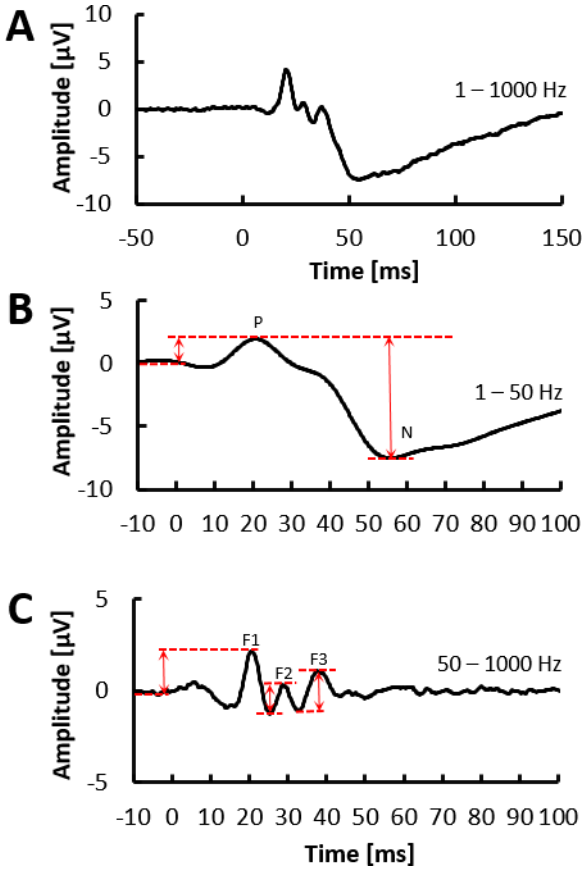

Figure 2. Evaluation of amplitudes for ppERG response waveform components. (A) Mean waveform recorded from 15 healthy eyes (11 right, 4 left) with viewing distance of 30 cm and mean ON-luminance of 1670 ph cd m^{-2}, 4.6 pattern RPS. Signals were recorded with passband 1 to 1000 Hz. (B) Isolated low-frequency components in the passband 1 to 50 Hz. Amplitude of the low-frequency positive component, P, was measured from baseline to peak. Amplitude of the low-frequency negative component, N, was measured as the difference between P and the subsequent trough. (C) Isolated high-frequency components in the passband 50 to 1000 Hz. Amplitudes of the three high-frequency peaks evaluated as illustrated (baseline to peak for F1, trough to peak for F2, trough to peak for F3).

Results

Comparison of ppERG and pERG Waveforms

To confirm that the custom-built peripheral pattern stimulus source elicited a response analogous to that obtained with conventional central-field pERG, responses were recorded using similar stimulus settings for both sources. Figure 3A plots the average ppERG (black) and pERG (green) waveforms obtained from six normally-sighted subjects when the mean ON-luminance and viewing distance

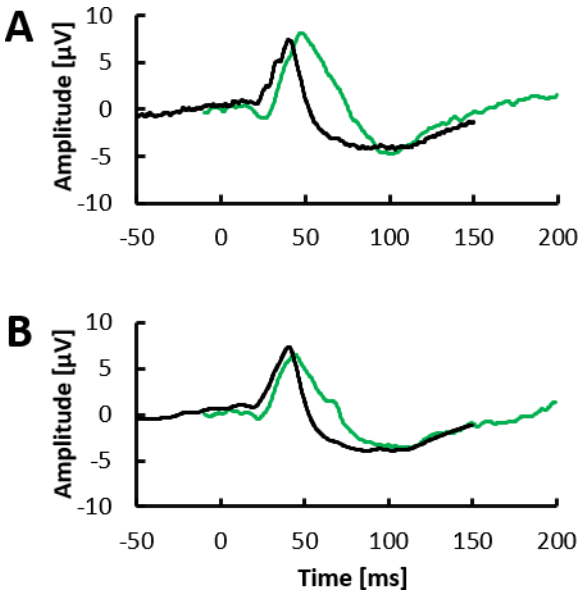

Figure 3. Comparison of ppERG and pERG response waveforms. Waveforms are average of six normally-sighted subjects. (A) Response waveforms for ppERG (black trace, 5° checks, 1- to 1000-Hz passband, field subtended 22°–50°) and pERG (green trace, 1° checks, 1- to 100-Hz passband, field subtended 0°–15°), with both systems set to approximately 4 RPS and mean ON-luminance of approximately 90 ph cd m^{-2}. (B) Response waveforms obtained when reversal rate (~4 rps), luminance (~90 ph cd m^{-2}), check size (5°) and passband (1–100 Hz) were matched; fields subtended as in panel A. *Black trace*, ppERG; *green trace*, pERG.

were matched (90 ph cd m^{-2} and 55 cm, respectively); at 55 cm, the ppERG stimulus falls in the mid-periphery (22°–50°, Fig. 1). The remaining stimulus difference was check size (5° for ppERG and 1° for pERG). Under these conditions, both the ppERG and pERG waveforms are dominated by early positive and later negative peaks, the primary differences being the earlier peak times, and "ripples" visible on the leading edge of the positive component, for the ppERG response.

To examine the effect of signal filtering, the average ppERG response in Figure 3A was digitally filtered to match the pERG passband (1–100 Hz), and replotted in Figure 3B (black trace); note the absence of high-frequency ripples on the leading edge. The green trace in Figure 3B is the pERG waveform obtained when the check size was increased to 5° to match the ppERG stimulus source. With luminance, check size, and signal filtering matched, the central and peripheral pERG waveforms are quite similar; the remaining differences are the slightly earlier positive component peak time, and the earlier and broader negative peak, for the ppERG responses. P in the average ppERG response occurs at 40.2 ms, and P50 in the average pERG response occurs at 44.0 ms; this 3.8 ms difference can be explained in part by the refresh rate of the pERG stimulus source (100 Hz), which adds 5 ms (one half of the duration of the display refresh) to reported implicit times.[23] The ppERG pattern reverses synchronously across the entire stimulus field.

Inter-Subject and Test–Retest Repeatability

Consistency across similar subjects, and test–retest repeatability for the same subject, are important considerations for efficacy of any test. Response waveforms from the 11 normally-sighted subjects (11 right eyes) are plotted in Figure 4A (black traces, red trace is average waveform). These responses were obtained with the viewing distance of 30 cm, mean ON-luminance of 1670 ph cd m^{-2}, and reversal rate of 4.6 RPS. There is a general similarity of waveform shape from subject to subject; this can be more clearly seen in Figures 4B and 4C, which plot the isolated low- and high-frequency components for each subject, respectively. The highest variability occurs in the amplitude of the N component, followed by F2; F2 showed a slight negative correlation with age (–0.06 μV $year^{-1}$, not shown), but N did not. Figure 4D plots the pERG responses recorded in the same subjects on the same days, for comparison (green trace is average waveform). Correlation between pERG P50 and ppERG P amplitudes was marginal ($r^2 = 0.55$), and was low between pERG N95 and ppERG N amplitudes ($r^2 = 0.05$).

The efficacy of a test is determined in part by the normal range, which in turn affects sensitivity and specificity. To compare normal ranges across different tests (of any modality or set of stimulus parameters), normalization of response variability to the mean is required. The means, SDs, and coefficients of variation (CV; SD ÷ mean) for the response feature values extracted from the Figure 4 waveforms are summarized in Table 2. The mean amplitudes for the main negative component in each test (pERG N95 and ppERG N) were not significantly different ($P = 0.11$, paired, two-tailed t-test), meaning that both pERG and ppERG have similar dynamic ranges when analyzed for the component that most directly reflects ganglion cell activity. Implicit times of P and N were significantly shorter than P50 and N95, respectively ($P < 0.001$). ppERG N amplitudes were more variable than pERG N95 amplitudes in this sample (CV = 34.2 and 23.4, respectively), but both were typical of ERG testing in general. Variabilities of

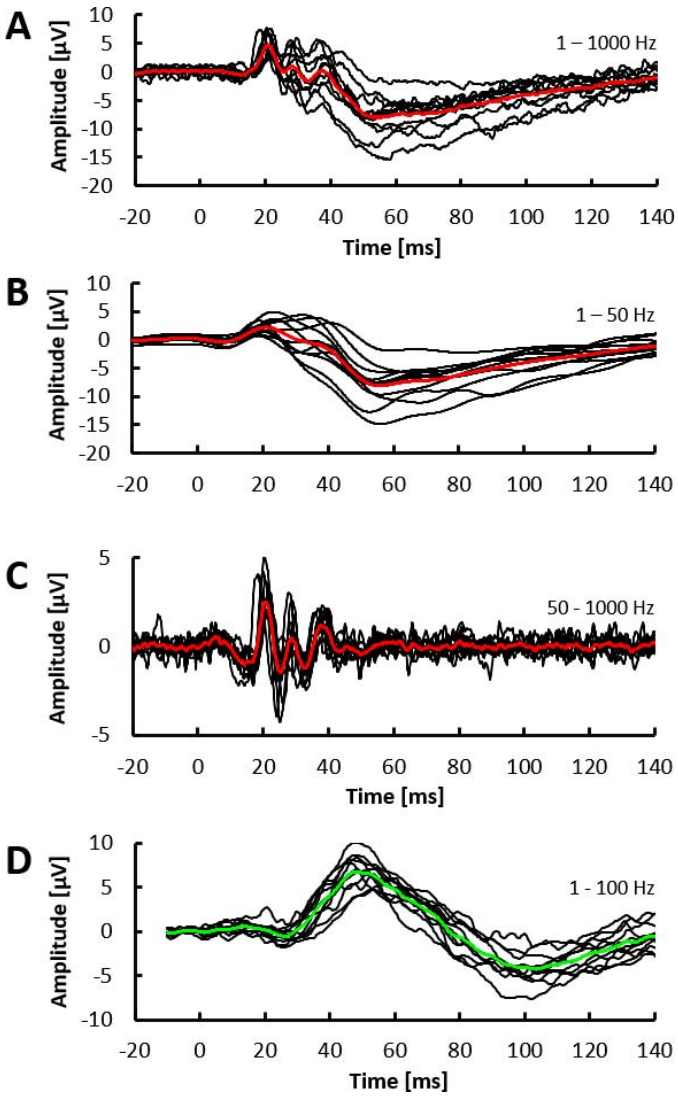

Figure 4. Waveform shape and variability in the ppERG response. (A) ppERG response waveforms recorded from 11 right eyes with viewing distance of 30 cm and mean ON-luminance of 1670 ph cd m^{-2}. *Red trace* is the average of the 11 black waveforms. (B) Isolated low-frequency components of the waveforms in (A). (C) Isolated high-frequency components of the waveforms in (A). (D) Conventional pERG responses, stimulus parameters as given in Table 1, same subjects as in (A). *Green trace* is the average of the 11 black waveforms.

implicit times of N and N95 were similar. Both pERG and ppERG yield response amplitudes measurable above noise levels in a clinically acceptable test time.

Repeatability for the ppERG response was examined. Figure 5A plots the response waveforms obtained from one subject on four different days, with retests done 5, 19, and 25 months after the initial test. Test–retest repeatability was very good; similar results were obtained in all six healthy subjects for which retest responses were obtained (3–19 months between tests, coefficient of determination between test and retest responses: $0.58 < r^2 < 0.98$). This degree of repeatability is encouraging for monitoring longitudinal changes in individuals. Intrasession repeatability is illustrated in Figure 5B, where each trace is the average response for a continuous 300 reversal run, with approximately 1-minute rest periods between runs. Correlation between ppERG responses obtained from left and right eyes of the same subject was also examined. Figure 5C plots the responses obtained from four different subjects (oculus sinster [OS] and oculus dexter [OD] responses obtained simultaneously). The correlation between pairs of eyes (OS versus OD) was high, with coefficient of determination between OS and OD responses $r^2 = 0.93 \pm 0.05$ (mean $\pm$ 1 SD); the correlation between right eyes (i.e., pairwise comparison between each eye and each of the other 3) was lower, $r^2 = 0.70 \pm 0.15$.

Parameters of the novel ppERG stimulus that could be varied were the mean ON-luminance, reversal rate, field subtended, and check size (confounded with viewing distance, as described below). These parameters were varied in a systematic way and the effects on the ppERG response components were analyzed.

Table 2. Amplitude and Implicit Time Values of Waveforms Shown in Figure 4

	Amplitude			Implicit Time		
	Mean (μV)	SD (μV)	CV (%)	Mean (ms)	SD (ms)	CV (%)
ppERG						
P	2.0	1.2	60.7	21.8	3.0	13.9
F1	2.9	1.0	33.6	20.9	0.8	4.0
F2	2.5	1.7	68.3	29.1	1.3	4.6
F3	2.7	0.9	34.4	38.1	1.3	3.4
N	9.5	3.3	34.2	56.9	3.5	6.1
pERG						
P50	6.1	1.3	21.2	50.4	3.5	6.9
N95	10.7	2.5	23.4	103.3	4.5	4.4

Luminance

Response waveforms obtained at a fixed viewing distance (55 cm) and reversal rate (4.6 RPS), and four different values for mean ON-luminance, are plotted in Figure 6. Figure 6A plots the mean waveforms

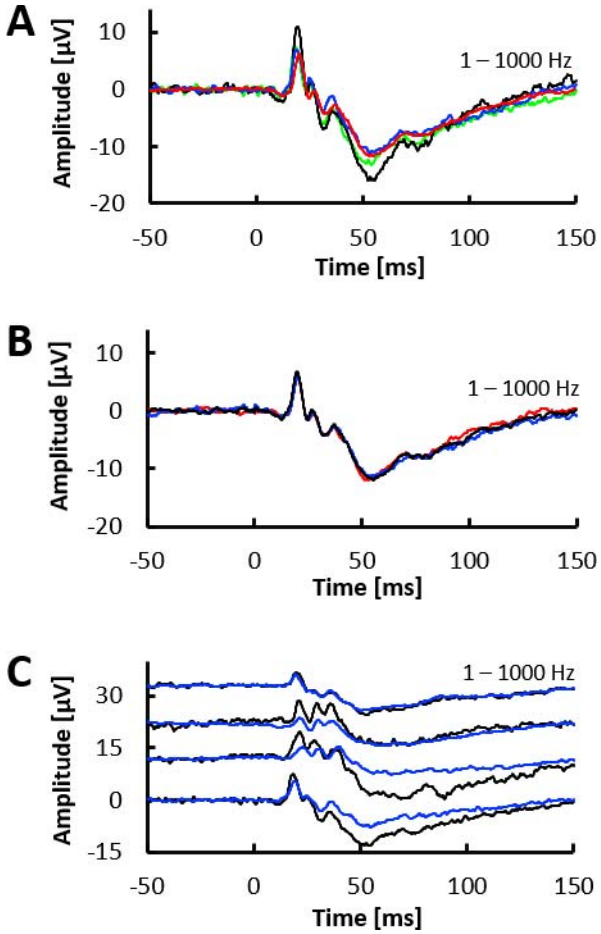

Figure 5. Test–retest variability, and left-right eye correlation. (A) ppERG response waveforms recorded in one subject on 4 different days. Responses plotted in *blue*, *green*, and *red* recorded 5, 19, and 25 months, respectively, after the response plotted in *black*. Responses obtained at a viewing distance of 30 cm and mean ON-luminance of 1670 ph cd m^{-2}. (B) Responses recorded in one subject, in one session. Each trace is the average of 300 reversals recorded continuously in one run, with approximately 1 minute between runs. (C) Responses obtained from right (*black*) and left (*blue*) eyes of four subjects, recorded simultaneously, stimulus conditions as in (A). Waveforms for three subjects offset vertically for clarity.

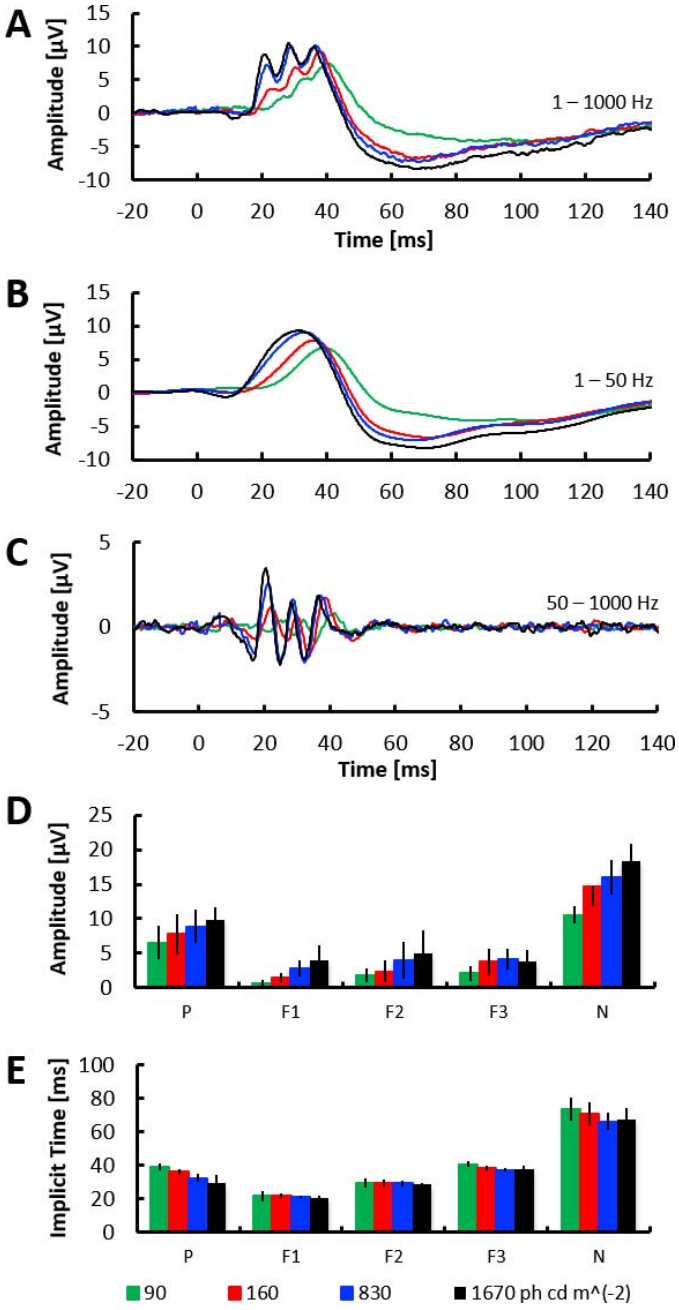

Figure 6. Effect of luminance on ppERG responses. Each waveform is the average response from six subjects; viewing distance fixed at 55 cm, reversal rate of 4.6 RPS. (A) Responses obtained when mean ON-luminance = 90 (*green*), 160 (*red*), 830 (*blue*), and 1670 (*black*) ph cd m^{-2}. (B) Isolated low-frequency components of the waveforms shown in (A). (C) Isolated high-frequency components of the waveforms shown in (A). (D) Response feature amplitudes for each luminance; bar heights plot mean, *error bars* plot ±1 SD. (E) Response feature implicit times for each luminance; bar heights plot mean, *error bars* plot ±1 SD.

obtained from six normally-sighted subjects; Figure 6B and 6C plot the isolated low- and high-frequency components, respectively. The effect of increasing luminance is most evident in the leading edge of the P component (likely preaxonal contribution), and in the evolution of the high-frequency components (F1–F3), with the strongest dependence shown by F1. These dependencies are summarized in Figure 6D. Implicit time for the P component became shorter at higher luminances, but the other components showed little dependence, as shown in Figure 6E.

Reversal Rate

Response waveforms at a fixed viewing distance (30 cm) and mean ON-luminance (1670 ph cd m^{-2}) were recorded at three reversal rates (2.3, 4.6, and 9.2 RPS); these responses are plotted in Figure 7. Figure 7A plots the mean waveforms obtained from six normally-sighted subjects; Figures 7B and 7C plot the isolated low- and high-frequency components, respectively. As reversal rate increased, P amplitude increased slightly, and N amplitude decreased significantly, –0.9 μV RPS^{-1} (linear regression, $r^2 = 0.91$); the fall-off of N amplitude is steeper than has been observed for N95 in conventional pERG (–0.3 μV RPS^{-1} over the range 2–7 RPS).[24] High-frequency ppERG response components were less sensitive to reversal rate over the range investigated; the greatest fall-off was seen for F2 between 4.6 and 9.2 RPS.

Check Size, Viewing Distance, and Field Subtended

Response waveforms obtained at a fixed mean ON-luminance (1670 ph cd m^{-2}) and reversal rate (4.6 RPS), and three different viewing distances, are plotted in Figure 8. Recall that viewing distance influences both the field subtended by the stimulus (visual angle and retinal area) and apparent check size (Fig. 1, Table 1). Figure 8A plots the mean waveforms obtained from six normally-sighted subjects; Figures 8B and 8C plot the isolated low- and high-frequency components, respectively. As the field subtended by the stimulus becomes more central (with increasing viewing distance), the amplitude of P increases, but the high-frequency components are nearly unchanged. These trends are summarized in Figure 8D. The N component peaks at approximately the same negative value for each distance (Fig. 8B), however the amplitude of N, which is measured from the peak of P, also increases with increasing viewing distance (Fig. 8D). Implicit times for P and N are shortest at the closest viewing distance, where the stimulus is presented farthest in the periphery (Fig. 8E).

To explore the effect of eccentricity of the stimulus, responses were recorded with a 4 × 4 check pattern (check size 10°, 4.6 RPS) presented in the central field, (subjects turned their head and fixated a target at the center of the 4 × 4 pattern, viewing distance maintained at 30 cm). These responses are compared with those elicited by the full pattern presented to the peripheral retina (i.e., normal fixation at the dome apex). The results are shown in Figure 9 for mean ON-luminances of 90 and 1670 ph cd m^{-2}. Wave-

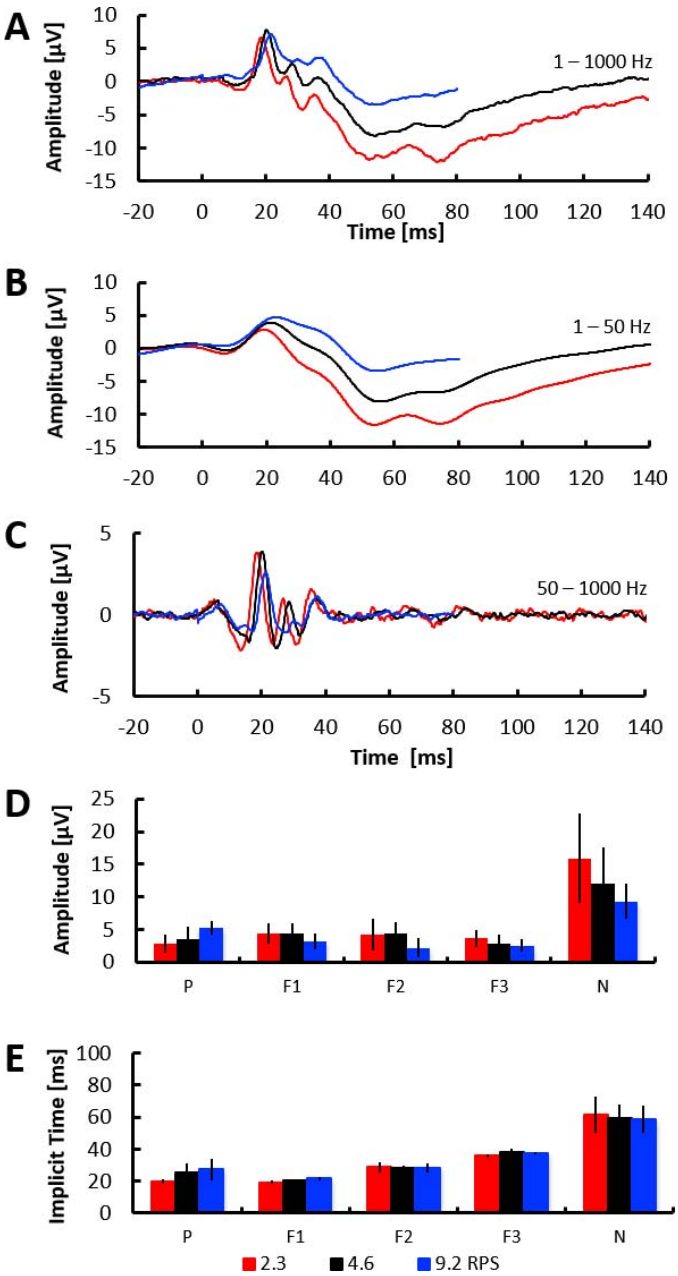

Figure 7. Effect of reversal rate on ppERG responses. Each waveform is the average response from six subjects; viewing distance of 30 cm, mean ON-luminance of 1670 ph cd m^{-2}. (A) Responses obtained for reversal rates of 2.3 (*red*), 4.6 (*black*), and 9.2 (*blue*) RPS. (B) Isolated low-frequency components of the waveforms shown in (A). (C) Isolated high-frequency components of the waveforms shown in (A). (D) Response feature amplitudes for each reversal rate; bar heights plot mean, *error bars* plot ±1 SD. (E) Response feature implicit times for each reversal rate; bar heights plot mean, *error bars* plot ±1 SD.

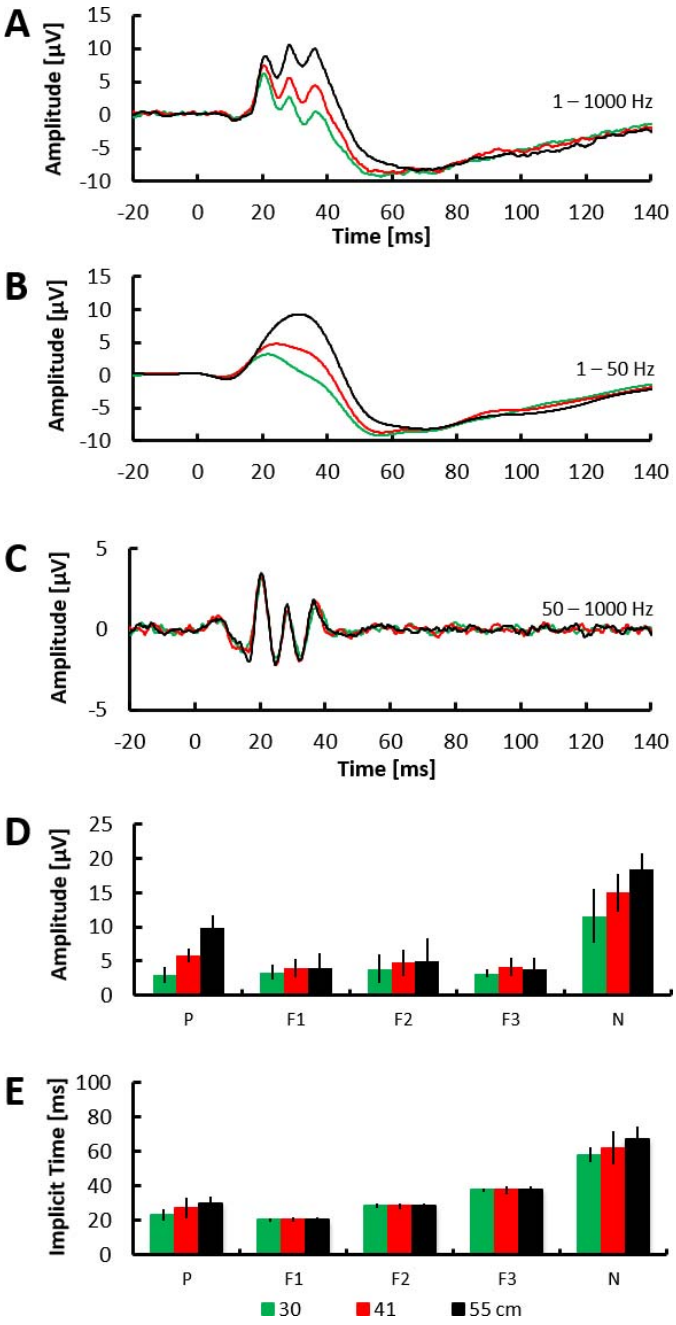

Figure 8. Effect of viewing distance on ppERG responses. Each waveform is the average response from six subjects; mean ON-luminance fixed at 1670 ph cd m^{-2}, reversal rate of 4.6 RPS. (A) Responses obtained when viewing distance = 30 cm (*green*), 41 cm (*red*), or 55 cm (*black*). (B) Isolated low-frequency components of the waveforms shown in (A). (C) Isolated high-frequency components of the waveforms shown in (A). (D) Response feature amplitudes for each viewing distance; bar heights plot mean, *error bars* plot ±1 SD. (E) Response feature implicit times for each viewing distance; bar heights plot mean, *error bars* plot ±1 SD.

forms plot the average response for six subjects; green traces plot pERG responses for comparison. At both luminances, the positive contribution to the waveform is significantly smaller with peripheral stimulation (red traces), allowing the N component to reach greater negative values (at earlier implicit times) with respect to baseline. This is consistent with the trend in Figure 8B, where the trailing edge of P (defined by a sum of positive and negative contributions) is most sensitive to eccentricity of the pattern. This suggests that with peripheral stimulation the N component is less corrupted by preaxonal corneal-positive contributions, and is more purely a reflection of axonal ganglion cell activity.[5]

Local Pattern Stimulation

Disease-related dysfunction in the retina is often sectoral rather than diffuse or global; for this reason, we evaluated local responses from peripheral retina in four field sectors. Average waveforms obtained from superior, nasal, inferior, and temporal quadrants of peripheral retina in nine right eyes are plotted in Figures 10A through 10C. For these tests, the stimulus source was moved to the nearest distance at which the entire stimulus was visible for all subjects (no part blocked by the bridge of the nose), which was 41 cm (Fig. 1D).

As seen Figure 10D, amplitude differences between sector responses are dramatic, with the largest P and N amplitudes from the temporal field, and the smallest from the nasal field, qualitatively consistent with temporal-nasal differences in ganglion cell density.[25] Sectoral responses allow for calculation of intrasubject ratios, which can reduce the influence of variance in absolute amplitude differences between subjects, and possibly highlight sectoral damage due to disease. The coefficient of variation for N amplitudes was 49% (average value across the four sectors, central bars of Fig. 10D). However, the CV for ratios of sector response amplitudes (where S', N', I', and T' represent the N amplitude of each sector divided by the sum of N amplitudes of the remaining three sectors) was reduced to 27%. This reduced intersubject variability demonstrates the narrowing of normative ranges when using intrasubject ratio values.

Discussion

Functional changes in the far peripheral retina are relatively under studied, in large part because of a lack of suitable tests. Full-field flash ERG probes the

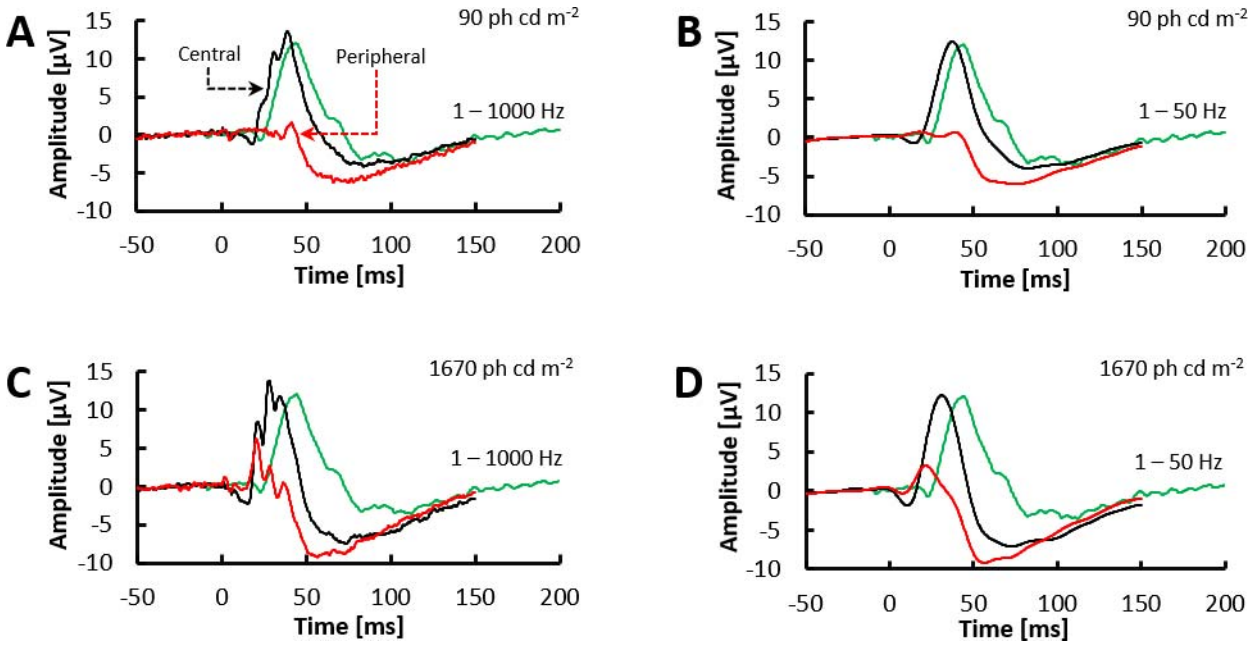

Figure 9. Effect of field subtended by a pattern stimulus. A reversing pattern was presented to the central field (4 × 4 checks viewed by altering direction of gaze) or peripheral field (full annular stimulus as in Fig. 1A) at a fixed viewing distance of 30 cm. Each waveform is the average response from six subjects. (A) ppERG response waveforms obtained with mean ON-luminance of 90 ph cd m^{-2}; central field response (*black*), peripheral field response (*red*). (B) Isolated low-frequency components of the waveforms shown in (A), colors as in (A). (C) ppERG response waveforms obtained with mean ON-luminance of 1670 ph cd m^{-2}; colors as in (A). (D) Isolated low-frequency components of the waveforms shown in (C), colors as in (A). In all panels, *green trace* plots response waveform from the pERG system with large 10° checks (90 ph cd m^{-2}, 30-cm viewing distance) for comparison.

entire retina, however local dysfunction in the periphery can have a relatively small effect on the response, resulting in amplitude changes that fall within the normal distribution. Goldmann perimetry can map the boundaries of the visual field, but is an indirect measure and suffers from poor repeatability. A dearth of objective tools for studying the peripheral retina, along with evidence of peripheral retina functional loss in early glaucoma, motivated the design of a pERG stimulus source that would enable convenient, objective measurement of ganglion cell function beyond 20° of visual angle. This novel system is now available to study inner retina functional changes in the peripheral retina, where ganglion cell diversity, density, morphology, orientation, and connectivity differ substantially from central retina.

The primary novel capability of the ppERG stimulus employed here is peripheral-field stimulation. With increasing eccentricity of the stimulus field, the positive contribution to the response waveform is reduced (Figs. 8, 9). In macaques, the pERG N95 component is eliminated in the presence of TTX block, while P50 is relatively unaffected.[5] Extending this finding to the human ppERG suggests that the negative component (N) is possibly a more pure reflection of axonal ganglion cell activity due to the lack of opposing corneal-positive contributions (recall that N is measured from the P peak). The reduced P component could be due to differences in the P source between central and peripheral retina, including cell density, cell type, and/or cell orientation. The anatomic axis of retinal neurons rotates approximately 90° from peripheral retina to central retina, and so the equivalent electrical dipole orientation for each cell also rotates, affecting how that cell contributes to the potential measured with a corneal electrode. This could also result in a relative increase in N contribution from the peripheral retina, where the axons and glia are oriented nearly perpendicular to their counterparts in the central retina.

Another novel capability of the ppERG stimulus employed here was the ability to present high-luminance patterns, with mean ON-luminance approximately 15× that achievable with standard pERG computer monitor sources. With increasing luminance, the ppERG response components become larger in amplitude (Fig. 6), including the evolution of high-frequency components not seen under ISCEV-recommended recording conditions. The high-frequency components of the ppERG response may be due to

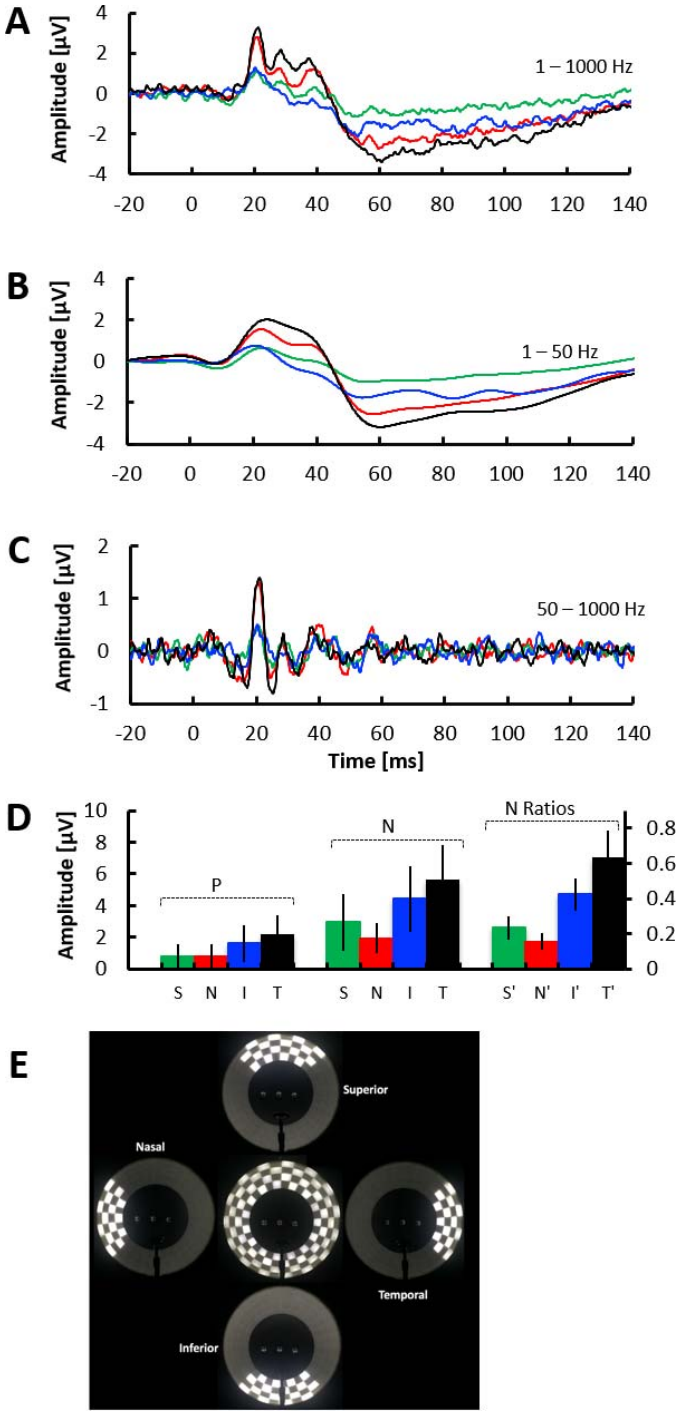

Figure 10. pERG responses evoked from sectors of peripheral retina. The 30 columns of the stimulus were divided into four sectoral stimuli to probe the superior (S), nasal (N), inferior (I), and temporal (T) fields. All tests done at a viewing distance of 41 cm, luminance of 1670 ph cd m^{-2}, and reversal rate of 4.6 RPS. (A) Mean waveforms from nine right eyes evoked by presenting the stimulus to each of the four sectors: superior (*blue*), nasal (*green*), inferior (*red*), and temporal (*black*). (B) Isolated low-frequency components of the waveforms shown in (A). (C) Isolated high-frequency components of the waveforms shown in (A). (D) Mean amplitudes of the P and N components recorded in each sector, *error bars* plot ±1 SD. *Right group* of bars plot the ratios of N amplitudes for each sector (see text); *error bars* plot ±1 SD. (E) Photographs of the sector stimuli, with the "all on" configuration shown in center; field designations for a right eye.

the light-adapted state during high-luminance pattern stimulation, similar to the dependence of flash ERG oscillatory potential (OP) amplitudes on light adaptation state.[26,27] However, even at moderate pattern luminance (90 ph cd s m^{-2}), modest high-frequency components were evoked from both peripheral and central retina when using relatively large 10° checks (Fig. 9A). Absence of high-frequency components in the conventional pERG response are most likely due to a combination of low-luminance pattern, modest level of light-adaptation, small check size, narrow recording bandwidth, and the low-pass filtering effect created by the long display refresh times. The robust and repeatable high-frequency components represent an objective source of information regarding the generator of these components, and thus deserve further investigation. It will be of interest to study the ppERG response in diabetic retinopathy patients with reduced flash ERG OP amplitudes.[28]

One consideration for ppERG testing is the effect of low acuity in the peripheral field. Contrary to ISCEV recommendations for pERG recording, no corrective lenses were worn during the ppERG test, regardless of prescription (with the exception of one contact lens wearer). Correction for refractive error in the far periphery would be challenging as the error varies with eccentricity. Fortunately, comparison of responses with and without correction showed minimal differences in response amplitudes (not shown), suggesting that the ppERG response is not strongly dependent on refractive error. This may be due in part to the relatively large check sizes used (5°–10°), and deserves further study. The optimum check size for detecting glaucoma with central patterns is approximately 1°, and falls off significantly with larger checks[2]; the optimal check size for peripheral patterns would be expected to be somewhat larger due to the larger average receptive fields for peripheral ganglion cells, and should be determined systematically.

An important potential advantage of the ppERG stimulus source used here is the ability to probe field sectors of the peripheral retina (Fig. 10). Probing local areas of retinal function has the potential to increase the sensitivity of any test, by increasing the effect size compared with healthy for localized dysfunction, and

by narrowing normal ranges through evaluation of relative values within an eye. Internally referenced measures have been used to increase the sensitivity of pERG,[29] perimetry,[30,31] OCT,[32,33] and flash ERG,[34] to sectoral functional and structural changes in glaucoma. Using an internally referenced measure of ppERG N amplitude yielded a coefficient of variation that was approximately one half of that seen with absolute N amplitudes; this approach should be explored in glaucoma where structural and functional changes are known to be sectoral.

As the pERG and ppERG tests probe different areas of the retina, the two tests may prove to be complementary, yielding superior sensitivity and specificity when results are strategically combined. The high sensitivity to glaucoma of steady-state pERG protocols such as PERGLA[35] and the pERG ratio[29] raise the possibility of added efficacy when employing high reversal rates in the periphery, and with a high-luminance pattern, though ppERG N amplitudes were largest with a relatively low reversal rate of 2.3 RPS (Fig. 7). The results summarized above motivate additional testing across a larger population of normally-sighted subjects, as well as patients with diseases that affect ganglion cell function, where the potential advantages of peripheral-field and high-luminance pattern stimuli can be more thoroughly evaluated.

Acknowledgments

The authors thank Heather Moss, MD, PhD, for helpful discussions during the preparation of this manuscript.

Supported by a University of Illinois at Chicago Chancellor's Innovation Fund Grant, and the National Institutes of Health Research Grants EY019510 (JJM) and EY001792 (University of Illinois at Chicago core grant) and an unrestricted departmental grant (Ophthalmology and Visual Sciences) from Research to Prevent Blindness.

S. Patangay, None; **Z. Derafshi**, None; **T. Vajaranant**, None; **J.C. Park**, None; **E. Ghahari**, None; **J.J. McAnany**, None; **J.R. Hetling**, None

References

1. Arden G, Vaegan, Hogg C. Clinical and experimental evidence that the pattern electroretinogram (pERG) is generated in more proximal retinal layers than the focal electroretinogram (FERG). *Ann NY Acad Sci*. 1982;388:580–601.
2. Bach M, Hiss P, Rover J. Check-size specific changes of pattern electroretinogram in patients with early open-angle glaucoma. *Doc Ophthalmol*. 1988;69:315–322.
3. Aldebasi Y, Drasdo N, Morgan J, North R. S-cone L+M-cone and pattern electroretinograms in ocular hypertension and glaucoma. *Vision Res*. 2004;44:2749–2756.
4. Hood D, Greenstein V, Frishman L, et al. Identifying inner retinal contributions to the human multifocal ERG. *Vision Res*. 1999;39:2285–2291.
5. Viswanathan S, Frishman L, Robson J. The uniform field and pattern ERG in macaques with experimental glaucoma: removal of spiking activity. *Invest Ophthalmol Vis Sci*. 2000;41:2797–810.
6. Miura G, Wang M, Ivers K, Frishman L. Retinal pathway origins of the pattern ERG of the mouse. *Exp Eye Res*. 2009;89:49–62.
7. Luo X, Frishman L. Retinal pathway origins of the pattern electroretinogram (PERG). *Invest Ophthalmol Vis Sci*. 2011;52:8571–8584.
8. Mafei L, Fiorentini A. Electroretinographic responses to alternating gratings before and after section of the optic nerve. *Science*. 1981;211:953–955.
9. Maffei L, Fiorentini A, Bisti S, Holländer H. Pattern ERG in the monkey after section of the optic nerve. *Exp Brain Res*. 1985;59:423–425.
10. Bach M, Hoffmann M. Update on the pattern electroretinogram in glaucoma. *Optom Vis Sci*. 2008;85:386–395.
11. Bach M, Poloschek C. Electrophysiology and glaucoma: current status and future challenges. *Cell Tissue Res*. 2013;353:287–296.
12. Bach M, Sulimma F, Gerling J. Little correlation of the pattern electroretinogram (PERG) and visual field measures in early glaucoma. *Doc Ophthalmol*. 1998;94:253–263.
13. Hood D, Xu L, Thienprasiddhi P, et al. The pattern electroretinogram in glaucoma patients with confirmed visual field deficits. *Invest Ophthalmol Vis Sci*. 2005;46:2411–2418.
14. Ventura L, Sorokac N, Santos R, Feuer W, Porciatti V. The relationship between retinal ganglion cell function and retinal nerve fiber thickness in early glaucoma. *Invest Ophthalmol Vis Sci*. 2006;47:3904–3911.
15. Sehi M, Pinzon-Plazas M, Feuer W, Greenfield D. Relationship between pattern electroretinogram, standard automated perimetry, and optic

nerve structural assessments. *J Glaucoma*. 2009; 18:608–617.
16. Banitt M, Ventura L, Feuer W, et al. Progressive loss of retinal ganglion cell function precedes structural loss by several years in glaucoma suspects. *Invest Ophthalmol Vis Sci*. 2013;54: 2346–2352.
17. Parisi V, Centofanti M, Gandolfi S, et al. Effects of coenzyme Q10 in conjunction with vitamin E on retinal-evoked and cortical-evoked responses in patients with open-angle glaucoma. *J Glaucoma*. 2014;23:391–404.
18. Parisi V, Centofanti M, Ziccardi L, et al. Treatment with citicoline eye drops enhances retinal function and neural conduction along the visual pathways in open angle glaucoma. *Graefes Arch Clin Exp Ophthalmol*. 2015;253:1327–1340.
19. Bach M, Pfeieffer N, Birkner-Binder D. Pattern-electroretinogram reflects diffuse retinal damage in early glaucoma. *Clin Vision Sci*. 1992;32:1219–1223.
20. Hood DC, Wang DI, Raza AS, de Morales CG, Liebmann JM, Ritch R. The locations of circumpapillary glaucomatous defects seen on frequency-domain OCT scans. *Invest Ophthalmol Vis Sci*. 2013;54:7338–7343.
21. Aylward GW, Vaegan, Billson FA. The wide-angle pattern electroretinogram. *Doc Ophthalmol*. 1990;73:275–283.
22. Graham, S, Wong V, Drance S, Mikelberg F. Pattern electroretinograms from hemifields in normal subjects and patients with glaucoma. *Invest Ophthalmol Vis Sci*. 1994;35:3347–3356.
23. Bach M, Brigell M, Hawlina M, et al. ISCEV standard for clinical pattern electroretinography (PERG): 2012 update. *Doc Ophthalmol*. 2012;126: 1–7.
24. Berninger T, Schuurmans RP. Spatial tuning of the pattern ERG across temporal frequency. *Doc Ophthalmol*. 1985;61:7–25.
25. Curcio CA, Allen KA. Topography of ganglion cells in human retina. *J Comp Neurol*. 1990;300:5–25.
26. Algvere P, Wachtmeister L. On the oscillatory potentials of the human electroretinogram in light and dark adaptation. II. effect of adaptation to background light and subsequent recovery in the dark. A Fourier analysis. *Acta Ophthalmol*. 1972; 50:837–862.
27. Benoit J, Lachapelle P. Light adaptation of the human photopic oscillatory potentials: Influence of the length of the dark adaptation period. *Doc Ophthalmol*. 1995;89:267–276.
28. Kizawa J, Machida S, Kobayashi T, Gotoh Y, Kurosaka D. Changes of oscillatory potentials and photopic negative response in patients with early diabetic retinopathy. *Jpn J Ophthalmol*. 2006;50:367–373.
29. Bach M, Ramharter-Sereinig A. Pattern electroretinogram to detect glaucoma: comparing the PERGLA and the PERG ratio protocols. *Doc Ophthalmol*. 2013;127:227–238.
30. Asman P, Heijl A. Glaucoma hemifield test: automated visual field evaluation. *Arch Ophthalmol*. 1992;110:812–819.
31. Johnson CA, Sample PA, Cioffi GA, Liebmann JR, Weinreb RN. Structure and function evaluation (SAFE): I. Criteria for glaucomatous visual field loss using standard automated perimetry (SAP) and short wavelength automated perimetry (SWAP). *Am J Ophthalmol*. 2002;134:177–185.
32. Um TW, Sung KR, Wollstein G, Yun S-C, Na JH, Schuman JS. Asymmetry in hemifield macular thickness as an early indicator of glaucomatous change. *Invest Ophthalmol Vis Sci*. 2012;53: 1139–1144.
33. Na JH, Kook MS, Lee Y, Yu SJ, Choi J. Detection of macular and circumpapillary structural loss in normal hemifield areas of glaucomatous eyes with localized visual field defects using spectral-domain optical coherence tomography. *Graefes Arch Clin Exp Ophthalmol* 2012;250:595–602.
34. Machida S, Tamada K, Oikawa T, Gotoh Y, Nishimura T, Kaneko M, Kurosaka D. Comparison of photopic negative response of full-field and focal electroretinograms in detecting glaucomatous eyes. *J Ophthalmol*. 2011;2011:pii: 564131.
35. Porciatti V, Ventura L. Normative data for a user-friendly paradigm for pattern electroretinogram recording. *Ophthalmology*. 2004;111:161–168.